J. Meas. Sci. Instrum., 2025, 16(1): 142-153.
DOI: 10.62756/jmsi.1674-8042.2025014
http://jmsi.publish.founderss.cn
jmsi@nuc.edu.cn

Galloping characteristics of catenary positive feeder considering aerodynamic damping

LI Yanzhe[1], JIN Xianglong[1], ZHAO Shanpeng[1*], ZHANG Youpeng[1], WANG Sihua[1], LI Wanrun[2]

1. School of Automatic and Electrical Engineering, Lanzhou Jiaotong University, Lanzhou 730070, China;
2. Electronic Technology Research Institute of Gansu Changfeng Elctronics Technology Co., Ltd., Lanzhou 730070, China

***Corresponding author:** ZHAO Shanpeng (zsp@mail.lzjtu.cn)

Received: October 18, 2023 **Revised:** January 20, 2024 **Accepted:** January 24, 2024

Abstract: The purpose of this study is to analyze the galloping characteristics of the catenary positive feeder in fluctuating wind areas considering dynamic-wind angle of attack and aerodynamic damping. Firstly, the flow field model of the catenary positive feeder was established, the fluctuating wind field was simulated by Davenport wind power spectrum and linear filtering method, and the wind speed at inlet in calculation domain was controlled by editing the profile file to simulate and calculate the aerodynamic characteristics of the positive feeder in the fluctuating wind area. Then, taking the positive feeder as the research object, the mathematical model of actual structure and the corresponding finite element model were established. By applying the wind load to the finite element model, the influence of aerodynamic damping caused by the self-movement of the positive feeder on the galloping response was analyzed, and the frequency domain characteristics of galloping displacement of the positive feeder considering aerodynamic damping were studied. Finally, the calculation method of aerodynamic damping by the *Guidelines for Electrical Transmission Line Structural Loading* (ASCE No.74) was used for the galloping response of the positive feeder and compared with the proposed method. The results show that when considering aerodynamic damping, the galloping amplitude of the positive feeder decreases significantly, and the first-order resonance effect on the vertical displacement and horizontal displacement decreases significantly. The galloping trajectories calculated by the two methods are consistent. Therefore, this study is of great significance to further clarify the ice-free galloping mechanism of the catenary positive feeder in violent wind areas.

Key words: positive feeder; aerodynamic damping; fluctuating wind area; galloping characteristics; nonlinear dynamic analysis

0 Introduction

Trains in violent wind areas are seriously affected by wind-induced disaster. To prevent train accidents, windbreak walls are usually built on one side along the railway. Consequently, wind speeds above windbreak walls increase, causing catenary positive feeders without icing to gallop[1-4]. Thus, the damage to relevant parts might be considerable, and conductors are prone to discharge and disconnection accidents, which seriously endangers the safety of train operation. In the galloping of catenary positive feeders, aerodynamic damping has a significant impact on it.

Many researchers have investigated the galloping characteristics of transmission lines of railways. For example, den Hartog[5] proposed a vertical excitation mechanism, Nigol et al.[6] proposed a torsional excitation mechanism based on it, and Yu et al.[7] proposed eccentric inertial coupling theory. Yan et al.[8] found that when the frequency ratio of in-plane modal to out-of-plane modal of iced four bundle conductors is approximately 2, its energy is constantly exchanged in motion. Ma et al.[9] tested six different types of iced conductors and analyzed the influence of turbulence on their aerodynamic characteristics. Based on vibration theory, Liu et al.[10] studied the influence of geometric parameters on the frequency of transmission line of railways as well as the influence of different modes on resonance effect. Fu et al.[11] established the calculation formula of torsional stiffness and verified its correctness by experiments.

The above researches focus on the galloping characteristics of iced conductors, and the corresponding conclusions are not suitable for the catenary positive feeder in violent wind areas. Due to the interference of windbreak walls on incoming wind, the catenary positive feeder is in the airflow growing area with a certain elevation angle,

which greatly changes the aerodynamic characteristics of the catenary positive feeder[12], making it gallop without icing and small span. Song[13] studied the aerodynamic characteristics of the catenary during icing and found that the vibration response of the catenary is different under different icing sections. In view of the influence of different sandy fractions on the aerodynamic characteristics of the positive feeder in a windy, sandy environment, the galloping amplitude of the positive feeder decreases significantly[14]. Since the above researches only consider the aerodynamic characteristics and galloping response of the catenary positive feeder in steady wind areas without considering aerodynamic damping, the actual galloping characteristics of the catenary positive feeder cannot be accurately analyzed.

In our work, the galloping characteristics of the catenary positive feeder considering aerodynamic damping in fluctuating wind areas were analyzed, and a dynamic equation whose damping term includes aerodynamic damping was established considering the relative movement between the positive feeder and the fluctuating wind. Based on this, a finite element model of single-span positive feeder was established, and the influence of aerodynamic damping on galloping response was simulated by ANSYS parametric design language (APDL) software. For comparative analysis, the results were compared with that in ASCE No.7[15]. After the galloping displacement was transformed by Fourier transform (FFT), the frequency domain characteristics of galloping response of the positive feeder considering aerodynamic damping could be concluded.

1 Dynamic equation of positive feeder considering aerodynamic damping

In case of the wind-induced galloping of positive feeders, the damping of the system dynamically increases, called aerodynamic damping [16]. Fig.1 shows the galloping diagram of the catenary positive feeder with single-span in violent wind areas.

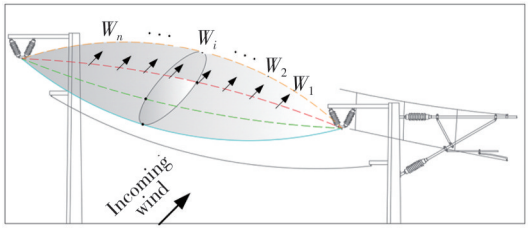

Fig. 1 Schematic diagram of multi-degree of freedom positive feeder galloping

Assuming that n degrees of freedom downwind galloping displacement of the single-span positive feeder is expressed as

$$\boldsymbol{W}=[W_1, W_2, \cdots, W_i, \cdots, W_n]^{\mathrm{T}}, \tag{1}$$

where $\boldsymbol{W}_i$ is the downwind galloping displacement of point i. Then, The structural dynamic equation of n degrees of freedom downwind displacement vectors of the positive feeder is expressed as

$$\boldsymbol{M}\ddot{\boldsymbol{W}}+\boldsymbol{C}_{\mathrm{sti}}\dot{\boldsymbol{W}}+\boldsymbol{K}_{\mathrm{T}}(\boldsymbol{W})\boldsymbol{W}=\boldsymbol{F}, \tag{2}$$

where $\boldsymbol{M}$ is the mass matrix, $\boldsymbol{C}_{\mathrm{sti}}$ is the stiffness damping matrix, $\boldsymbol{W}$ is the displacement matrix, $\boldsymbol{K}_{\mathrm{T}}(\boldsymbol{W})$ is a stiffness substitution matrix considering geometric nonlinearity, and $\boldsymbol{F}$ is the fluctuating wind load matrix of the positive feeder. To analyze the galloping characteristics, the fluctuating wind load on the positive feeder is mainly divided into resistance $\boldsymbol{F}_{\mathrm{D}}$ and lift $\boldsymbol{F}_{\mathrm{L}}$.

The tangent stiffness matrix is expressed as

$$\boldsymbol{K}_{\mathrm{T}}(\boldsymbol{W})=\boldsymbol{K}_{\mathrm{L}}+\boldsymbol{K}_{\mathrm{N}}(\boldsymbol{W})+\boldsymbol{K}_{\sigma}(\boldsymbol{W}), \tag{3}$$

where $\boldsymbol{K}_{\mathrm{L}}$ and $\boldsymbol{K}_{\mathrm{N}}(\boldsymbol{W})$ are linear and nonlinear stiffness matrix, respectively; and $\boldsymbol{K}_{\sigma}(\boldsymbol{W})$ is the stress stiffening matrix.

During the movement of the positive feeder under fluctuating wind load, its static-wind angle of attack, relative movement and dynamic-wind angle of attack are shown in Fig.2.

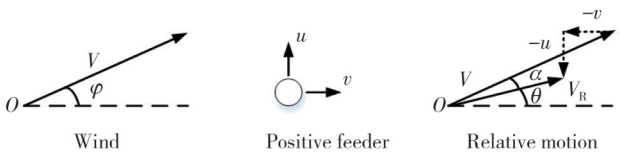

Fig. 2 Schematic diagram of dynamic wind angle of attack

In Fig.2, V is the wind speed; u and v are the vertical and horizontal movement speeds at the positive feeder, respectively; V_{R} is the wind speed considering relative movement; and φ is the wind angle of attack when relative movement is not considered, θ is the dynamic-wind angle of attack considering relative movement, $\alpha=\varphi-\theta$.

Without considering the relative movement between the positive feeder and the fluctuating wind, the fluctuating wind load on the positive feeder is expressed as

$$\begin{aligned}F_{\mathrm{D}}=&\frac{1}{2}\rho C_{\mathrm{D}}[A_1(\bar{u}_{z,1}+\tilde{u}_1)^2,\cdots,\\&A_i(\bar{u}_{z,i}+\tilde{u}_i)^2,\cdots,A_n(\bar{u}_{z,n}+\tilde{u}_n)^2]^{\mathrm{T}},\end{aligned} \tag{4}$$

$$\begin{aligned}F_{\mathrm{L}}=&\frac{1}{2}\rho C_{\mathrm{L}}[A_1(\bar{u}_{z,1}+\tilde{u}_1)^2,\cdots,\\&A_i(\bar{u}_{z,i}+\tilde{u}_i)^2,\cdots,A_n(\bar{u}_{z,n}+\tilde{u}_n)^2]^{\mathrm{T}},\end{aligned} \tag{5}$$

where ρ is the air density; C_{L} and C_{D} are the lift and resistance coefficients of the positive feeder, respectively; and $\bar{u}_{z,i}$, $\tilde{u}_i$ and A_i are the average wind speed, the fluctuating wind speed, and the windward

area at point i of the positive feeder, respectively.

When considering the relative movement between the positive feeder and the fluctuating wind, the fluctuating wind load is calculated by

$$\boldsymbol{F}_{\mathrm{D}}=\frac{1}{2}\rho C_{\mathrm{D}}[A_1(\bar{u}_{z,1}+\tilde{u}_1-\dot{W}_1)^2,\cdots,A_i(\bar{u}_{z,i}+\tilde{u}_i-\dot{W}_i)^2,\cdots,A_n(\bar{u}_{z,n}+\tilde{u}_n-\dot{W}_n)^2]^{\mathrm{T}}, \quad (6)$$

$$\boldsymbol{F}_{\mathrm{L}}=\frac{1}{2}\rho C_{\mathrm{L}}[A_1(\bar{u}_{z,1}+\tilde{u}_1-\dot{W}_1)^2,\cdots,A_i(\bar{u}_{z,i}+\tilde{u}_i-\dot{W}_i)^2,\cdots,A_n(\bar{u}_{z,n}+\tilde{u}_n-\dot{W}_n)^2]^{\mathrm{T}}. \quad (7)$$

Substituting Eqs. (6) and (7) into Eq. (2), we can get

$$\boldsymbol{M}\ddot{\boldsymbol{W}}+(\boldsymbol{C}_{\mathrm{sti}}+\boldsymbol{C}_{\mathrm{aero}})\dot{\boldsymbol{W}}+\boldsymbol{K}_{\mathrm{T}}(\boldsymbol{W})\boldsymbol{W}=\boldsymbol{F}_{\mathrm{D1}}+\boldsymbol{F}_{\mathrm{D2}}, \quad (8)$$

where

$$\boldsymbol{F}_{\mathrm{D1}}=\frac{1}{2}\rho C_{\mathrm{D}}[A_1(\bar{u}_{z,1}+\tilde{u}_1)^2,\cdots,A_i(\bar{u}_{z,i}+\tilde{u}_i)^2,\cdots,A_n(\bar{u}_{z,n}+\tilde{u}_n)^2]^{\mathrm{T}}, \quad (9)$$

$$\boldsymbol{F}_{\mathrm{D2}}=\frac{1}{2}\rho C_{\mathrm{D}}\left[A_1\dot{W}_1{}^2,\cdots,A_i\dot{W}_i{}^2,\cdots,A_n\dot{W}_n{}^2\right]^{\mathrm{T}}. \quad (10)$$

In Eq. (10), $\boldsymbol{F}_{\mathrm{D2}}$ is the square term of movement speed of the positive feeder, and $\boldsymbol{C}_{\mathrm{aero}}$ is the aerodynamic damping matrix caused by the relative movement of positive feeder, that is

$$\boldsymbol{C}_{\mathrm{aero}}=\rho C_{\mathrm{D}}\mathrm{diag}[A_1(\bar{u}_{z,1}+\tilde{u}_1),\cdots,A_i(\bar{u}_{z,i}+\tilde{u}_i),\cdots,A_n(\bar{u}_{z,n}+\tilde{u}_n)], \quad (11)$$

$$\boldsymbol{M}\ddot{\boldsymbol{W}}+(\boldsymbol{C}_{\mathrm{str}}+\boldsymbol{C}_{\mathrm{aero}})\dot{\boldsymbol{W}}+\boldsymbol{K}_{\mathrm{T}}(\boldsymbol{W})\boldsymbol{W}=\boldsymbol{F}_{\mathrm{L1}}+\boldsymbol{F}_{\mathrm{L2}}, \quad (12)$$

where

$$\boldsymbol{F}_{\mathrm{L1}}=\frac{1}{2}\rho C_{\mathrm{L}}[A_1(\bar{u}_{z,1}+\tilde{u}_1)^2,\cdots,A_i(\bar{u}_{z,i}+\tilde{u}_i)^2,\cdots,A_n(\bar{u}_{z,n}+\tilde{u}_n)^2]^{\mathrm{T}}, \quad (13)$$

$$\boldsymbol{F}_{\mathrm{L2}}=\frac{1}{2}\rho C_{\mathrm{L}}\left[A_1\dot{W}_1{}^2,\cdots,A_i\dot{W}_i{}^2,\cdots,A_n\dot{W}_n{}^2\right]^{\mathrm{T}}. \quad (14)$$

In Eq. (14), $\boldsymbol{F}_{\mathrm{L2}}$ is the square term of the motion speed of the positive feeder, and $\boldsymbol{C}_{\mathrm{aero}}$ is the aerodynamic damping matrix caused by the relative movement of the positive feeder, that is

$$\boldsymbol{C}_{\mathrm{aero}}=\rho C_{\mathrm{L}}\mathrm{diag}[A_1(\bar{u}_{z,1}+\tilde{u}_1),\cdots,A_i(\bar{u}_{z,i}+\tilde{u}_i),\cdots,A_n(\bar{u}_{z,n}+\tilde{u}_n)]. \quad (15)$$

It can be seen from Eqs. (11) and (15) that the size of the aerodynamic damping matrix $\boldsymbol{C}_{\mathrm{aero}}$ is related to the wind speed at the positive feeder. Since the wind speed at each point of the transmission line is positive, the damping of the whole system increases with the increase of the aerodynamic damping $\boldsymbol{C}_{\mathrm{aero}}$.

2 ASCE No. 74 aerodynamic damping equation

American Society of Civil Engineers (ACSE) No. 74 have provided the calculation method of aerodynamic damping, and the aerodynamic damping of positive feeder is calculated by

$$\xi_{\mathrm{a}}=0.000\,048\left(\frac{\bar{u}_{10}}{f_{\mathrm{w}}\left(\frac{d}{12}\right)}\right)C_{\mathrm{f}}, \quad (16)$$

where $\bar{u}_{10}$ is the average wind speed at 10 m; d is the diameter; C_{f} is the shape coefficient; and f_{w} is the fundamental frequency of out of plane oscillation as

$$f_{\mathrm{w}}=\left[\frac{1}{sag}\right]^{0.5}, \quad (17)$$

where sag is the mid-span radian.

Since wind force 8 and 9 days in violent wind areas are usually more than 200 days throughout the year, after consulting the wind grade table, the average wind speed $\bar{u}_{10}=20\ \mathrm{m\cdot s^{-1}}$ at 10 m is taken, and ξ_a is 0.071 3 from Eq. (16). When solving the nonlinear motion equation of the positive feeder, the damping matrix $\boldsymbol{C}$ is calculated by

$$\boldsymbol{C}=\alpha\boldsymbol{M}+\beta\boldsymbol{K}, \quad (18)$$

where $\boldsymbol{M}$ and $\boldsymbol{K}$ are the mass matrix and the stiffness matrix, respectively; α and β are determined by the total damping ratio ξ of the structure and the first two order basis rates ω_1 and ω_2, respectively, that is

$$\alpha=\xi\frac{2\omega_1\omega_2}{\omega_1+\omega_2}, \quad (19)$$

$$\beta=\xi\frac{2}{\omega_1+\omega_2}. \quad (20)$$

When using the aerodynamic damping calculation method from ASCE No. 74 to solve the galloping response of the positive feeder, the influence of aerodynamic damping on the galloping characteristics of the positive feeder is directly considered, here ξ_{s} is taken as 0.005, and $\xi=\xi_{\mathrm{s}}+\xi_{\mathrm{a}}$.

3 Simulation and experiment

3.1 Simulation of fluctuating wind

The fluctuating wind in structural wind engineering indicates that the fluctuating wind is decomposed into average component and fluctuating component[17]. The fluctuating wind at any point is expressed as

$$u_{z,i}=\bar{u}_{z,i}+\tilde{u}_i. \quad (21)$$

According to the natural geographical environment in the strong wind areas, the fluctuating wind can be simulated based on the Davenport spectrum as

$$S_v(f)=\frac{4k\bar{u}_{10}^2}{f}\cdot\frac{\zeta^2}{(1+\zeta^2)^{\frac{4}{3}}},\tag{22}$$

where

$$\zeta=\frac{600f}{\pi\bar{u}_{10}},$$

$S_v(f)$ is the power spectrum of fluctuating wind, $\bar{u}_{10}$ is the wind speed at 10 m high, f is the circular frequency, and k is the ground roughness coefficient. Combined with the actual landform in the violent wind area, it is set to 0.005 in this study.

The linear filtering method describing the statistical characteristics of time series is selected to simulate the fluctuating wind. The research shows that the fourth-order autoregressive model has high accuracy. Therefore, it is selected to simulate the fluctuating wind field[18]. The flow chart of fluctuating wind simulated by the linear filtering method is shown in Fig.3.

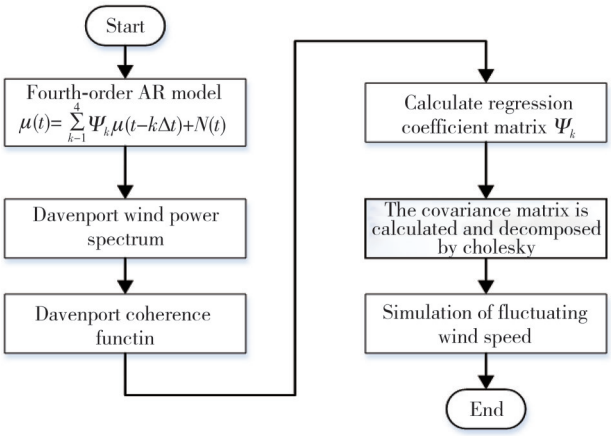

Fig. 3 Flow chart of fluctuating wind simulation

According to the above method, the time history of the fluctuating wind with an average wind speed of 10 m·s^{-1} is generated, as shown in Fig.4. Fig.5 shows the comparison between the simulated spectrum and the target spectrum, here the Davenport coherence function is adopted to calculate the target value. It can be seen that the target value of the fluctuating wind is consistent with the simulated value, indicating that the fluctuating wind can well reflect the distribution characteristics of fluctuating energy in the frequency domain.

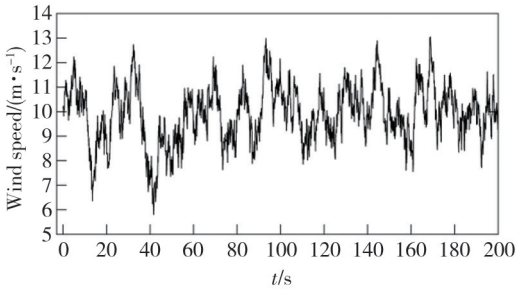

Fig. 4 Time history of fluctuating wind

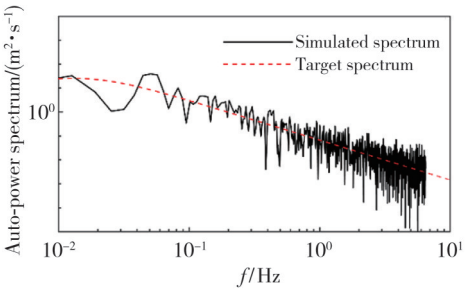

Fig. 5 Comparison of power spectra

3.2 Aerodynamic characteristics of positive feeder in fluctuating wind field

The two-dimensional wind field model of the actual positive feeder is established. The calculation domain is 23.8 m long and 15 m high, with the embankment slope of 1∶1.5 and the height of the windbreak wall of 3.5 m. Dividing the grid in calculation domain, the model is shown in Fig.6. Extracting the data from 20 s fluctuating wind, editing the profile file, and controlling the wind speed at a time interval of 0.1 s, the formats are shown as

((inlet transient 201 0)
(time [0:0.1:20])
(v_x [feng su]))

where [feng su] is the matrix for the data of 20 s fluctuating wind speed.

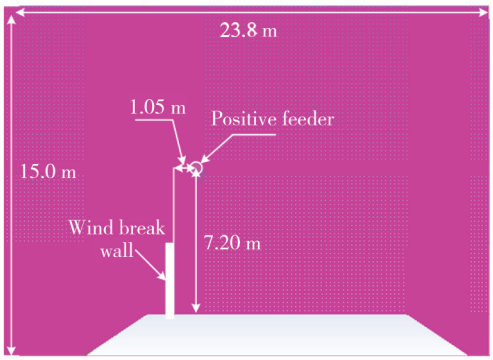

Fig. 6 Computational model with grids

The wind field of the positive feeder is calculated, with the time step of 0.01 s and the average wind speed of 10 m·s^{-1}. The time history of the wind speed at the inlet is shown in Fig.7, the wind speed nephogram in the wind field at the positive feeder is shown in Fig.8, and the time history of wind speed at the positive feeder is shown in Fig.9, and time history of angle of attack from static wind at the positive feeder is shown in Fig.10. It can be seen from Fig.8 that the wind speed at the positive feeder increases significantly when the wind at the inlet is blocked and accelerated by the windbreak wall. From the vertical and horizontal components of the wind speed at the positive feeder shown in Fig.9, the time history of

the angle of attack from the static wind at the positive feeder shown in Fig.10 can be obtained.

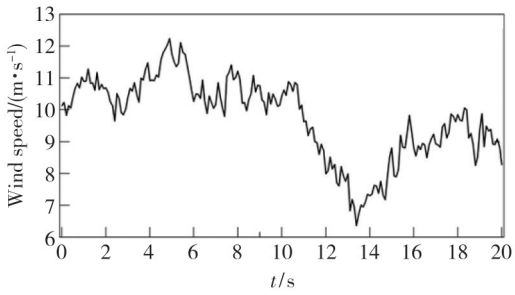

Fig. 7 Time history of wind speed at inlet

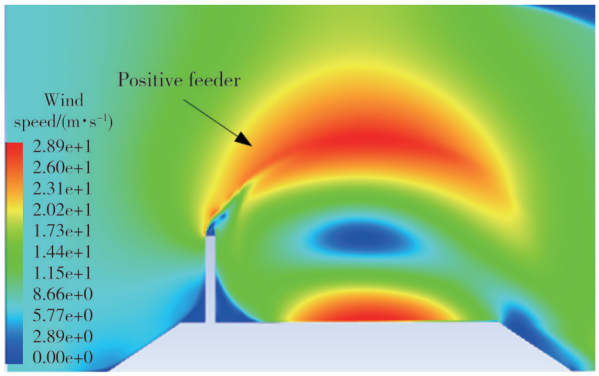

Fig. 8 Wind speed nephogram at positive feeder

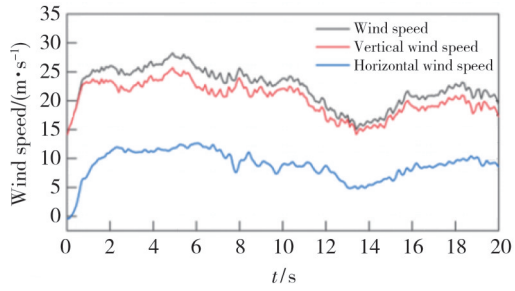

Fig. 9 Time history of wind speed at positive feeder

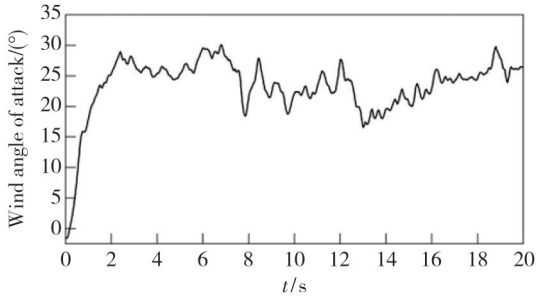

Fig. 10 Time history of angle of attack of static wind

The two-dimensional wind field model of the positive feeder is established and meshed. The grid height of the first layer near the wall of the positive feeder is determined by the dimensionless number $y+$. To accurately simulate the aerodynamic characteristics on the surface of the positive feeder, the settings are as follows: Transition SST flow field model, SIMPLEC algorithm, second-order discrete pressure equation, a time step of 0.005 s, 4 000 calculation steps, and simulation time of 20 s. The time histories of the lift and resistance coefficients at the positive feeder in the fluctuating wind field with an average wind speed of 10 $m \cdot s^{-1}$ are obtained, as shown in Figs. 11 and 12, respectively. Combined with the time history of wind speed at the positive feeder, the lift and resistance coefficients at the positive feeder fluctuates due to the change of wind speed at the positive feeder.

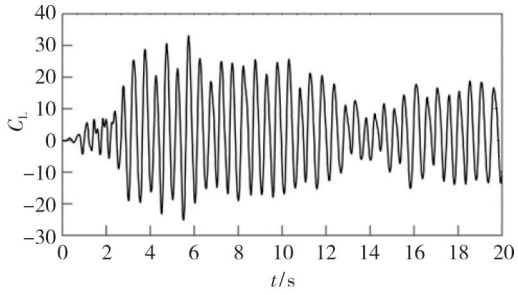

Fig. 11 Time history of positive feeder lift coefficient

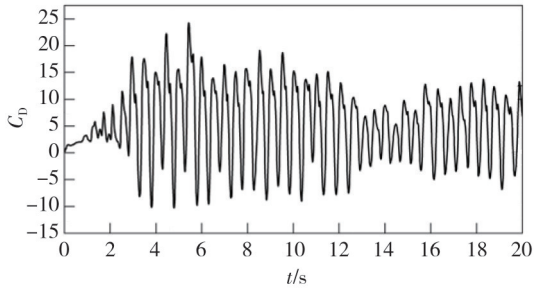

Fig. 12 Time history of positive feeder drag coefficient

3.3 Wind tunnel test

The wind tunnel model of the positive feeder with a similarity ratio of 1:59 was designed, as shown in Fig.13. By adjusting the fan frequency, the wind speed at the inlet changed, and the wind speeds at the positive feeder at different inlet wind speeds were measured by the anemometer, as shown in Fig. 14. The wind speeds measured by the wind tunnel test are compared with the simulation results by flow field model, as listed in Table 1.

Fig. 13 Wind tunnel test model

It can be seen from Table 1 that the errors of wind speed between the measured results and the simulation results at the positive feeder are small. Considering the airtightness

of the device and other factors, the errors are within the allowable range. The wind speed obtained from the test and simulation is about twice the wind speed at the inlet, which means that the established calculation model of fluctuating wind field can accurately reflect the wind speed at the positive feeder in the actual environment. Therefore, the simulation of the fluctuating wind field is feasible, which provides a reliable basis for studying the aerodynamic characteristics of the full-scale model of the positive feeder.

Fig. 14 Anemometer

Table 1 Experimental and simulation results of wind speed

Inlet wind speed/(m•s^{-1})	Wind speed at positive feeder/(m•s^{-1})	
	Experiment	Simulation
5.18	11.31	11.29
7.55	16.42	16.46
10.14	22.05	22.10
13.03	28.27	28.41
14.88	32.38	32.44
16.54	36.11	36.07
18.76	40.79	40.87

Since the galloping of the overhead catenary positive feeder is the most violent when the angle between the transmission line and the incoming wind is vertical in violent wind areas, the following study focuses on the galloping response of the positive feeder when the wind blows vertically to the transmission line.

4 Finite element model and dynamic characteristics of positive feeder

4.1 Finite element model of positive feeder

The positive feeder (LGJ-300/25) of the catenary in the violent wind area is an overhead conductor with a standard span of 50 m, with a calculated section of 333.31 mm^2, a calculated diameter of 23.76 mm, an elastic modulus of 65 GPa, and a mass of 1 058 kg·km^{-1}. The catenary positive feeder has a flexible clue structure that only bears tension. Therefore, the link10 element in ANSYS is selected to simulate the positive feeder in this study. In the APDL three-dimensional coordinates system, the finite element model of the positive feeder is established with x axis, y axis, and z axis representing the transmission line direction, vertical direction, and horizontal direction, respectively. When performing a nonlinear calculation on the positive feeder, the options of stress stiffness and large deformation in ANSYS are turned on. In this study, the catenary equation is used to find the shape of the positive feeder. The catenary equation is[20]

$$Y=\frac{H}{q}\left[\mathrm{ch}\alpha-\mathrm{ch}\left(\frac{2\beta X}{L}-\alpha\right)\right], \tag{23}$$

where $\alpha=\mathrm{sh}^{-1}\left[\beta\frac{C}{L}\right]+\beta$, $\beta=\frac{qL}{2H}$, Y is sag, H is the horizontal tension, q is the dead weight load of conductor, L is the span, X is the horizontal distance from the suspension point to the calculation point, and C is the height difference of hanging points at both ends of the positive feeder.

The finite element model of the positive feeder is evenly divided into 200 elements, and 201 coordinates of finite element nodes are obtained. Susbstituting the parameters of the catenary positive feeder into Eq. (23), the form-finding analysis of the positive feeder under the dead weight load can be carried out to obtain its static characteristics. The calculation results show that the theoretical value of sag in the middle span of the positive feeder is 0.95 m, and the sag of node 102 in the middle span of the positive feeder in the finite element model is 0.950 03 m, with the error of 0.003%. The correctness of the finite element model is verified.

4.2 Dynamic characteristics of positive feeder

To analyze the galloping characteristics of the positive feeder, the modal analysis of the positive feeder with finite element model is needed to calculate its low-order natural frequency and vibration mode. Since the tension is applied at both ends of the model after the form-finding of the positive feeder is completed, resulting in large geometric deformation of the positive feeder, the large-deformation prestressed modal analysis method from ANSYS software is adopted. Table 2 shows the natural frequencies and vibration modes of the first three modes of the positive feeder. It can be seen that the first-order natural frequencies of single-span positive feeder equal in plane and out of plane, and the second-order and the third-order natural frequencies are close. The first three modes are a one-half wave, two half-waves, and three half-waves, respectively, which are consistent in plane and out of plane.

Table 2 First three modes of positive feeder

Order	Direction	Natural frequency/Hz	Vibration mode
First order	In plane	0.547 2	
	Out of plane	0.547 2	
Second order	In plane	1.092 4	
	Out of plane	1.094 2	
Third order	In plane	1.505 5	
	Out of plane	1.641 6	

5 Analysis of galloping response

5.1 Force analysis of positive feeder

When the positive feeder is moving, the angle of attack from wind will change with the movement of the conductor. Combined with the angle of attack from dynamic wind to the positive feeder, the stress analysis of the positive feeder in the wind axis coordinate system is shown in Fig.15. Lift F_l and drag F_d are calculated by

$$F_l = \frac{1}{2}\rho_{air}U^2 DC_L, \tag{24}$$

$$F_d = \frac{1}{2}\rho_{air}U^2 DC_D, \tag{25}$$

where ρ_{air} is the air density, D is the peripheral diameter of catenary positive feeder, C_L is the lift coefficient, and C_D is the drag coefficient.

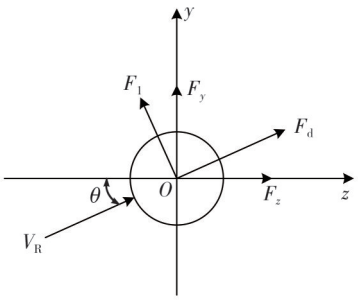

Fig. 15 Force analysis of positive feeder

The horizontal component and vertical component of the positive feeder under fluctuating wind load are calculated respectively by

$$F_z = F_d\cos\theta - F_l\sin\theta, \tag{26}$$

$$F_y = F_l\cos\theta + F_d\sin\theta. \tag{27}$$

5.2 Galloping response considering aerodynamic damping

The 20 s fluctuating wind load calculated by simulation in the fluctuating wind field is loaded into 201 nodes of the finite element model in the form of the horizontal component and vertical component as Eqs. (26) and (27) respectively, and the displacement iteration calculation is carried out at the end of the previous time step, taking into account the angle of attack from dynamic wind and aerodynamic damping of the positive feeder. Applying two kinds of fluctuating wind loads calculated by Eqs. (4) — (7) to the finite element model, the corresponding galloping amplitudes are calculated and compared, which reveals the effect of aerodynamic damping on the galloping response of positive feeder.

The catenary positive feeder in violent wind areas is in V-type suspension mode, and the suspension device remains stable when galloping. The positive feeders between spans have little influence each other due to the small span of 50 m, and the the largest galloping displacement is in the middle of span. Therefore, the mid-span galloping characteristics of a single-span positive feeder can represent the galloping characteristics of the positive feeder in the whole transmission line. Fig.16 shows the time history of vertical displacement and horizontal displacement in the middle of span of the positive feeder with and without aerodynamic damping, respectively. It can be seen that when aerodynamic damping is not considered, the lowest point of galloping in the vertical direction is -0.608 m, and the highest point of galloping in the vertical direction is 1.548 m, with the vertical amplitude of 2.156 m. The leftmost coordinate in the horizontal direction is —0.256 m, the rightmost coordinate in the horizontal direction is 1.072 m, with the horizontal amplitude of 1.328 m. Considering the aerodynamic damping, the lowest point in the vertical direction is —0.072 m, and the highest point is 1.364 m, with the vertical amplitude of 1.436 m, which is 0.72 m lower than that without aerodynamic damping. The leftmost coordinate in the horizontal direction is 0.192 m, the rightmost coordinate is 0.964 m, with the horizontal amplitude of 0.772 m, which is 0.556 m less than that without considering aerodynamic damping. It also can be observed that the galloping amplitude of the positive feeder decreases significantly when considering the angle of attack and aerodynamic damping from dynamic wind.

According to the calculation method of aerodynamic damping provided by ASCE No.74, combined with the first two natural frequencies based on the modal analysis, the following results can be obtained ξ_a, 0.071 33; ξ, 0.071 83; α, 0.052 375; and β, 0.087 619. Then, the time history diagram of displacement in vertical and horizontal directions of positive feeder is obtained, as shown in Fig. 17. Considering the aerodynamic damping, in the vertical direction, the lowest point of galloping is —0.032 m, the highest point is 1.280 m, with the maximum amplitude of 1.312 m, which is 0.844 m less than that without considering aerodynamic damping. In the horizontal direction, the leftmost point of galloping is 0.296 m, the rightmost

point is 0.908 m, with the maximum amplitude of 0.612 m, which is 0.716 m less than that without considering aerodynamic damping. It can also be observed that considering aerodynamic damping, the difference between the vertical displacement amplitude and the calculated result is 0.124 m, and the difference between the horizontal displacement amplitude and the calculated result is 0.160 m. In contrast, without considering aerodynamic damping, the galloping amplitude of positive feeder also decreases significantly.

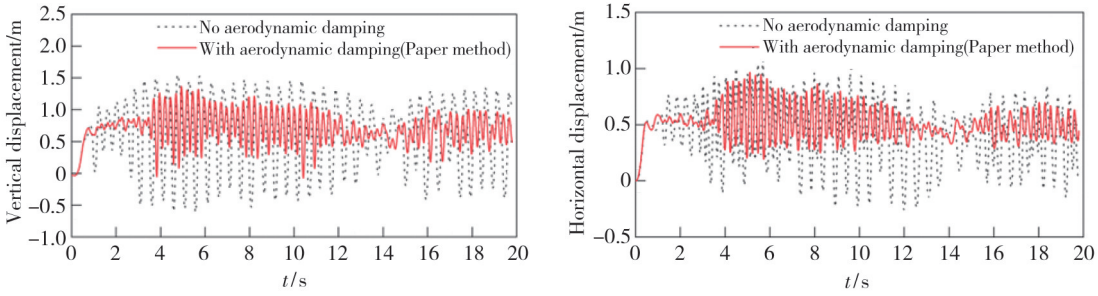

(a) Vertical direction (b) Horizontal direction

Fig. 16 Time history of mid-pan displacement using proposed method

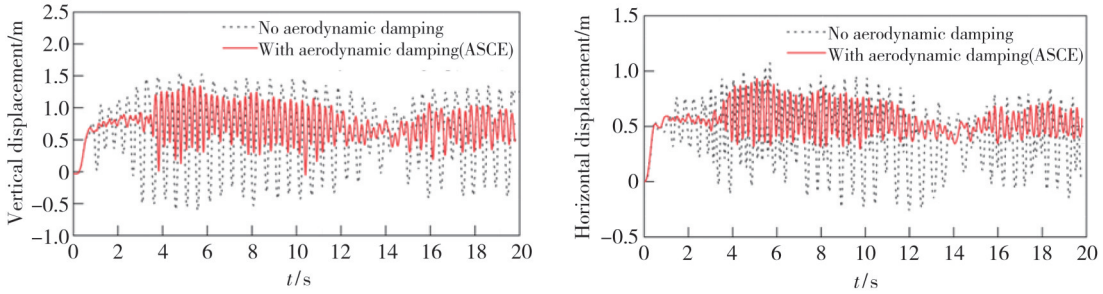

(a) Vertical direction (b) Horizontal direction

Fig. 17 Time history of mid-span displacement by the method of ASCE No. 74

Fig. 18 shows the galloping trajectory of the positive feeder using the aforementioned two calculation methods without considering aerodynamic damping and considering aerodynamic damping, respectively. It can be observed that the galloping amplitude of the positive feeder considering aerodynamic damping is significantly lower than that without considering aerodynamic damping, whereas the galloping trajectories considering aerodynamic damping are relatively consistent in amplitude. As shown in Figs.18(b) and (c), considering the relative movement between the positive feeder and the fluctuating wind, the galloping trajectory with the proposed method is highly consistent with the ellipse, and the galloping trajectory obtained by ASCE No.74 is flatter and similar to the arc. According to the actual galloping monitoring video and simulation analysis, the actual galloping trajectory of the positive feeder is oval[21]. Therefore, compared with the galloping trajectory obtained by ASCE No. 74, the galloping trajectory of the positive feeder obtained by the proposed method is more consistent with that in the actual environment. Combined with the galloping trajectory in Fig.18(a), it can be seen that the results considering the aerodynamic damping are more in line with the actual situation when calculating the galloping response of the positive feeder.

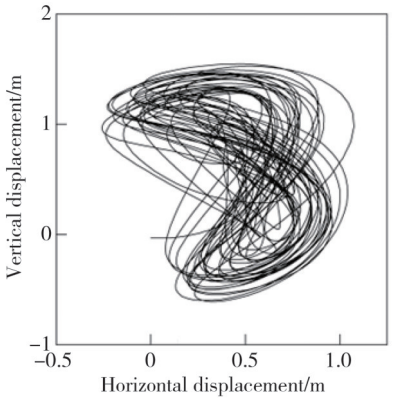

(a) Without considering aerodynamic damping

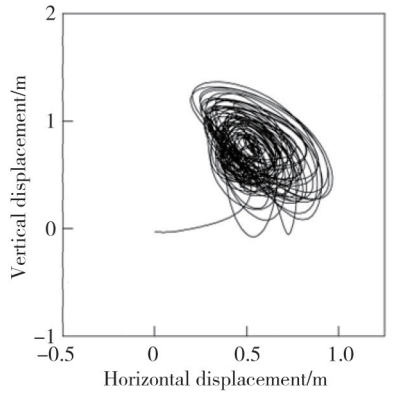

(b) Proposed method considering aerodynamic damping

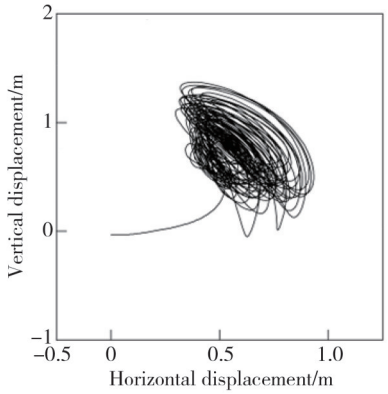

(c) ASCE No. 74 considering aerodynamic damping

Fig. 18 Mid-span galloping trajectory

5.3 Frequency domain analysis of galloping characteristics

As for the galloping characteristics of conductors, the vibration frequency f of the conductor is usually close to the first several natural frequencies f_n of the conductor, which is calculated by[22]

$$f=f_n=\frac{n}{2L}\sqrt{\frac{T}{m}}, \tag{28}$$

where n is the vibration order, L is the span, T is the conductor tension, and m is the mass per unit length of positive feeder.

Since the wind-induced vibration of the positive feeder is mainly the first-order vibration mode, the resonance effect easily occurs at the first two natural frequencies. Therefore, according to Eq. (28) and relevant data, the first two natural frequencies are 0.55 Hz and 1.1 Hz, respectively. Fourier transform (FFT) is performed on the galloping displacement trajectory of the positive feeder to obtain the corresponding displacement spectrum. When aerodynamic damping is not considered, the vertical displacement spectrum and horizontal displacement spectrum in the middle of span of the positive feeder are shown in Fig.19. The galloping mode of the positive feeder is determined by analysis of the galloping displacement spectrum. According to the modal analysis, the first-order natural frequency is 0.547 2 Hz, and the second-order natural frequency is 1.092 4 Hz. Compared with the first-order natural frequency of 0.55 Hz and the second-order natural frequency of 1.1 Hz calculated by Eq. (28), when aerodynamic damping is not considered, the first two major frequencies of 0.537 4 Hz and 1.087 Hz in the displacement spectrum of the positive feeder are consistent with the first two natural frequencies caluculated by the above two calculation methods. It can be known that when aerodynamic damping is not considered, the mid-span galloping form of the positive feeder is dominated by the first-order vibration mode in the vertical direction and by the first-order and second-order vibration modes in the horizontal direction, respectively. As shown in Fig. 18(a), it can also be verified that the galloping form of the positive feeder is consistent with that by spectrum analysis without considering the galloping trajectory of aerodynamic damping.

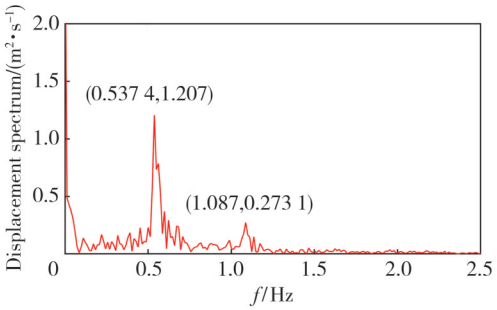

(a) Vertical displacement spectrum

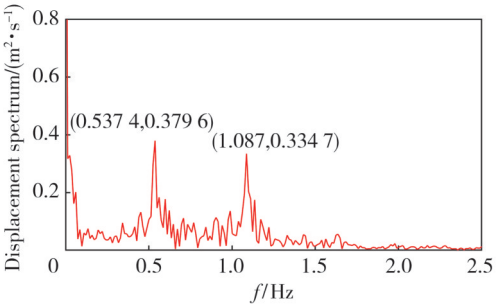

(b) Horizontal displacement spectrum

Fig. 19 Mid-span displacement spectrum without considering aerodynamic damping

The research on structural vibration shows that the galloping response of the positive feeder is composed of a background component and a resonance component. The background component is concentrated in the low-frequency part of the displacement spectrum, while the resonance component is concentrated near the low-order natural vibration frequency of the structure. It can be seen from Figs.18 and 19 that when aerodynamic damping is not considered, the galloping amplitude of the positive feeder increases significantly compared with that when aerodynamic damping is considered. The main peak frequency of the mid-span displacement spectrum in the vertical direction is 0.537 4 Hz, which is very close to the first-order natural frequency of in-plane positive feeder, and the resonance effect in the vertical direction is very strong. The two peak frequencies of the horizontal displacement spectrum are 0.537 4 Hz and 1.087 Hz, respectively, which are respectively close to the first two natural frequencies of 0.547 2 Hz and 1.094 2 Hz out of

plane of the positive feeder. The resonance effect in the horizontal direction is also very strong. It can be seen from Fig.19 that when aerodynamic damping is not considered, the main peak values of the displacement spectrum in the vertical direction and horizontal direction of the positive feeder are 1.207 Hz and 0.379 6 Hz, respectively. It can also be seen that the resonance effect in the vertical direction is significantly stronger than that in the horizontal direction. In Fig. 16, when the aerodynamic damping is not considered, the galloping amplitudes of the positive feeder in the vertical and horizontal directions increase by 0.720 m and 0.556 m respectively compared with that when the aerodynamic damping is considered. It is further verified that when the aerodynamic damping is not considered, the resonance effect of the positive feeder in the vertical direction is stronger than that in the horizontal direction. Fig.20 and Fig.21 are the mid-span displacement spectra of the positive feeder considering aerodynamic damping. It can be observed that the resonance component of the mid-span galloping response of the positive feeder decreases obviously. In the vertical and horizontal directions, the resonance component near the first-order natural frequency is close to 0, and the resonance effect almost disappears. When using the aerodynamic damping calculation provided by ASCE No.74, the displacement spectrum obtained is in good agreement with that obtained by proposed method.

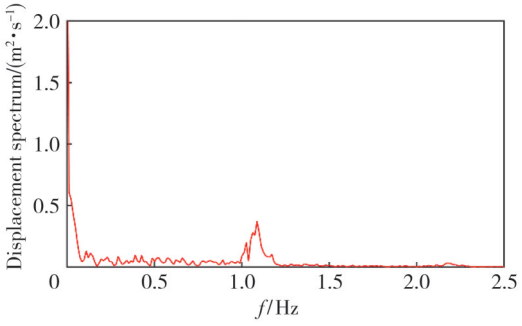

(a) Vertical displacement spectrum

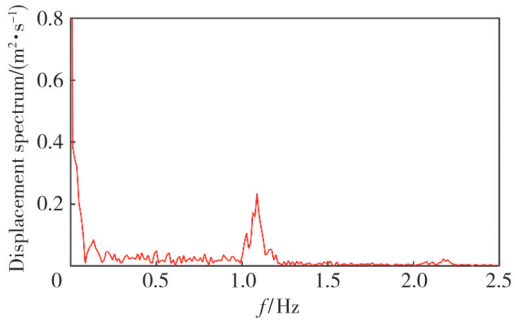

(b) Horizontal displacement spectrum

Fig. 20 Mid-span displacement spectrum considering aerodynamic damping

Under the excitation of fluctuating wind load, the relative movement between the positive feeder and the incoming flow causes the aerodynamic damping of the dynamic system, and the positive feeder always moves relative to the fluctuating wind in the process of galloping. Therefore, aerodynamic damping is common when the catenary positive feeder gallops. When calculating the galloping response of catenary positive feeder, the influence of the first-order resonance component on the galloping response of catenary positive feeder can be ignored.

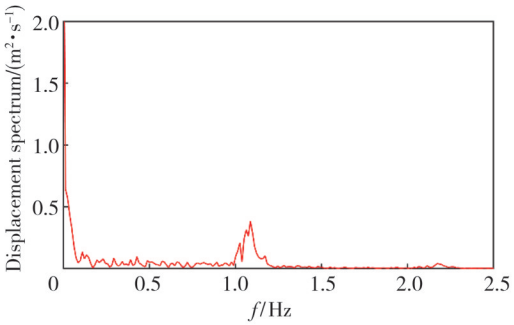

(a) Vertical displacement spectrum

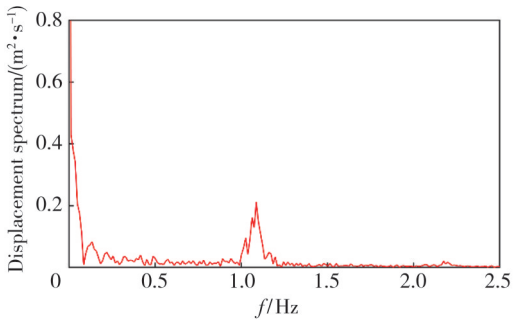

(b) Horizontal displacement spectrum

Fig. 21 Mid-span displacement spectrum considering aerodynamic damping (ASCE No. 74)

6 Conclusions

1) This study focuses on the influence of aerodynamic damping and dynamic wind angle of attack caused by the relative movement between the positive feeder and the incoming flow on the galloping. The aerodynamic damping increases the overall damping of the system and significantly reduces the galloping amplitude of the positive feeder. Compared with the case without considering the aerodynamic damping, the maximum galloping amplitudes in the vertical and horizontal directions of the positive feeder span are reduced by 0.72 m and 0.556 m, respectively, indicating that the aerodynamic damping factor in the galloping response calculation cannot be ignored.

2) The calculated result of galloping amplitude using the method from ASCE No.74 considering aerodynamic damping is consistent with that by proposed method.

However, the galloping trajectory obtained by the proposed method is more consistent with the actual trajectory of the positive feeder.

3) Compared with the mid-span galloping trajectory of the positive feeder considering aerodynamic damping effect and that without considering aerodynamic damping, the spectral peak disappears at the first-order natural frequency in the vertical direction. In the horizontal direction, the resonance effect is significantly weakened from one half-wave and two half-waves to one half-wave.

4) In the actual galloping process of the positive catenary feeder, the aerodynamic damping caused by the relative movement between the positive feeder and the fluctuating wind always exists. The first-order resonance effect will not occur in the galloping process of the positive feeder. Therefore, the first-order resonance effect between the positive feeder and pulsating wind can not be considered in the galloping calculation of the positive feeder.

Acknowledgement

This work was supported by National Natural Science Foundation of China (No.51867013), and Natural Science Foundation of Gansu Province (No.20JR5RA414).

Declaration of conflicting interests

The authors have no conflict of interests related to this publication.

References

[1] HUANG S L. Research on wind protection standard of Lanzhou-Urumqi high-speed railway. Journal of Railway Engineering, 2019, 36(6): 14-17.

[2] XIAO J H, YAO Z Y, QU J J, et al. Characteristics and formation mechanism of extreme wind conditions in the 100 mile wind area of Lanzhou-Urumqi Railway. China Railway Science, 2016, 37(3): 130-137.

[3] MENG X L, LI K, XIE S B, et al. Characteristics of wind conditions and wind protection engineering design partition in the windy area of Lanzhou-Urumqi high-speed railway. China Desert, 2018, 38(5): 972-977.

[4] PAN X M, MA X Q, XU J. Analysis andevalua tion of the windproof effect of the Lanzhou-Xinjiang high speed rail wind-break wall. Journal of Arid Meteorology, 2019, 37(3): 496-499.

[5] den HARTOG J P. Transmission line vibration due to sleet. Transactions of the American Institute of Electrical Engineers, 1932, 51(4): 1074-1076.

[6] NIGOL O, BUCHAN P G. Conductor galloping part I - den HARTOG mechanism. IEEE Transactions on Power Apparatus and Systems, 2007, 100(2): 699-707.

[7] YU P, SHAH A H, POPPLEWELL N. Inertially coupled galloping of iced conductors. Journal of Applied Mechanics, 1992, 59(1): 140-145.

[8] YAN B, LIU X H, ZHAO L, et al. Nonlinear galloping of iced four bundle conductors with internal resonance. Applied Mathematics and Mechanics, 2014, 35(1): 39-49.

[9] MA W Y, GU M, QUAN Y, et al. Experimental study on aerodynamic characteristics of quasi elliical iced conductor. Journal of Tongji University (Natural Science Edition), 2010, 38(10): 1409-1413.

[10] LIU X H, HU Y, YAN B, et al. Analysis of in-plane dynami characteristics and resonance conditions of multi-stage conductors. Vibration and Shock, 2018, 37(18): 18-29.

[11] FU G J, WANG L M, GUAN Z C, et al. Analysis of torsional stiffness and galloping mechanism of overhead transmission line bundle conductor. High Voltage Technology, 2013, 39(5): 1001-1010.

[12] ZHANG Y P, WANG T, ZHAO S P, et al. Influence of wind-break wall on aerodynamic characteristics of positive feeder of overhead contact line of Lanzhou- Xinjiang high-speed railway. Journal of Railway Science and Engineering, 2019, 16(7): 1628-1636.

[13] SONG Y. Study on dynamic current collection charac teristics of high speed railway pantograph catenary under ambient wind. Chengdu: Southwest Jiaotong University, 2018: 28-33.

[14] YUE Y W. Research on the influence of wire surface roughness on galloping response of catenary positive feeder under wind and sand environment. Lanzhou: Lanzhou Jiaotong University, 2021.

[15] American Society of Civil Engineers. Guidelines for Electrical Transmission Line Structural Loading: ASCE 74-2015. Reston: American Society of Civil Engneers, 2015.

[16] SOUZA L. The behavior of transmission lines under high wind. Ontario: The University of Western Ontario, 1996.

[17] YUAN B, YING H Q, XU J W. Simulation of fluctuating wind speed based on linear filtering method and implementation of Matlab program. Structural Engineer, 2007, 4(5): 55-61.

[18] HOU F G. Dynamic response analysis of Ferris wheel structure under wind load. Shanghai: Shanghai Jiao Tong University, 2014.

[19] LEI J M, TAN Z M. Numerical simulation for flow around circular cylinder at high Reynolds number based on Transition SST model. Journal of Beijing University of Aeronautics and Astronautics, 2017, 43(2): 207-217.

[20] WANG X M. Numerical analysis of engineering struc ture with ANSYS. Beijing: People's Communications Press, 2007: 467-471.

[21] ZHANG Y P, ZHAO S X, ZHAO S P, et al. Design of on-line monitoring system for galloping of cate-nary positive feeder in strong wind area of Lanxin high speed railway. Journal of the China Railway, 2021, 43(7): 57-65.

[22] ZHANG Y P, ZHANG C R, ZHAO S P, et al.

Antigalloping effectiveness analysis of catenary positive feeder cable-stayed insulator in strong wind section of Lanzhou Xinjiang high speed railway. High Voltage Technology, 2020, 46(11): 3905-3913.

计及气动阻尼效应的接触网正馈线舞动特性

李彦哲[1], 金相龙[1], 赵珊鹏[1*], 张友鹏[1], 王思华[1], 李万润[2]

1. 兰州交通大学 自动化与电气工程学院, 甘肃 兰州 730070;
2. 甘肃长风电子科技有限责任公司 电子技术研究所, 甘肃 兰州 730070

摘　要： 本研究分析脉动风场下计及动态风攻角与气动阻尼的接触网正馈线舞动特性。首先，建立实际尺寸的接触网正馈线流场模型，利用Davenport风功率谱以及线性滤波法模拟脉动风场，并通过编辑Profile文件控制计算域入口风速，仿真计算脉动风场下正馈线气动特性。其次，建立接触网正馈线结构动力学数学模型与有限元模型，并对正馈线有限元模型施加风荷载，仿真分析正馈线自身运动引起的气动阻尼对其舞动响应的影响，研究计及气动阻尼的正馈线舞动位移的频域特性，同时与ASCE No. 74中计算气动阻尼方法进行对比。结果表明，考虑气动阻尼效应时正馈线舞动幅值显著减小，竖直位移与水平位移一阶共振效应明显减弱，两种方法计算所得舞动轨迹较吻合。本研究对于进一步明确大风区接触网正馈线无覆冰舞动机制具有重要的意义。

关键词： 接触网正馈线；气动阻尼；脉动风场；舞动特性；非线性动力分析

引用格式： LI Yanzhe, JIN Xianglong, ZHAO Shanpeng, et al. Galloping characteristics of catenary positive feeder considering aerodynamic damping. Journal of Measurement Science and Instrumentation, 2025, 16(1): 142-153. DOI: 10.62756/jmsi.1674-8042.2025014